Journal of Power Sources, 47 (1994) 63–78

An electrochemical study of PEO:$LiBF_4$-glass composite electrolytes

Binod Kumar and Jeffrey D. Schaffer
University of Dayton Research Institute, Dayton, OH 45469-0170 (USA)

Munichandraiah Nookala* and Lawrence G. Scanlon, Jr.
Wright Laboratory, Aero Propulsion and Power Directorate, Wright-Patterson Air Force Base, OH 45433 (USA)

(Received December 7, 1992; accepted in revised form June 9, 1993)

Abstract

Several solid electrolytes derived from poly(ethylene oxide) doped with lithium tetrafluoroborate and a high conductivity lithium borosulfate glass were formulated and investigated for their electrochemical performance. The electrochemical characterization included a.c. impedance measurements, the temperature dependence of conductivity, scanning electron microscopy (SEM), cyclic voltammetry (CV), and the charge/discharge cycling of symmetric cells. The ionic conductivities of these electrolytes at ambient temperature were around 10^{-7} S cm^{-1}. Although no significant improvement in conductivity was observed, the cyclic voltammetry, impedance spectroscopy, and cycling data on Li/polymer/Li and Li/polymer/Ni cells reveal that the electrode reactions are facilitated by the glass incorporation.

Introduction

A great deal of interest in solid polymer electrolytes has developed in the last decade [1]. The major driving force for the interest is a potential technological application–rechargeable power sources with long cycle life. Justifiable research efforts have made significant advances in the state of understanding of solid polymer electrolytes. These efforts have also identified certain issues such as ambient temperature conductivity, cationic transport number, electrode–electrolyte interfacial reactions and lithium recycleability. It is apparent that these issues must be addressed and resolved before solid polymer batteries become a commercial reality.

In the last three years, two approaches to enhance the room temperature conductivity of polymer composite electrolytes have been reported. The first approach makes use of a high conducting liquid phase in a polymer matrix [2], frequently referred to as gel electrolytes. Due to the presence of a liquid phase, these electrolytes exhibit room temperature conductivity in the 10^{-2} to 10^{-3} S cm^{-1} range. The basis of the second approach is an incorporation of solid inorganic additives or fillers in the conducting polymers [3, 4]. An enhancement of conductivity occurs at low temperatures, however, the conductivity of this type of solid electrolyte material is not as high as those made by the first approach. Basically, both approaches produce composite electrolyte materials,

*National Research Council Fellow.

the difference being the fact that the gel type electrolyte consists of a solid polymer and a highly conductive liquid phase whereas in the second type of electrolyte both the polymer and the inorganic additive are solids. As pointed out in the preceding paragraph, in addition to high conductivity, the electrolytes should exhibit minimal reactivity with lithium and mechanical resilience in order to commercially produce rechargeable lithium batteries with a long cycle life. The basic kinetic arguments suggest that the reactivity of lithium will be less with a solid–solid composite electrolyte as compared to a solid–liquid composite electrolyte. In fact, there is some experimental evidence supporting this hypothesis [5]. It is therefore believed that the very high and appealing conductivity of gel type electrolytes may have limited use, so in order to advance solid polymer battery technology, the second approach deserves further attention. Thus, the objective of this paper is to explore and evaluate the electrochemical properties of polymer–inorganic solid composite electrolytes. A lithium borosulfate glass was chosen as the inorganic solid phase due to its relatively high lithium ion conductivity [6] at room temperature.

Experimental

Polyox N750* was used as the source of poly(ethylene oxide). The Polyox material was doped with reagent grade lithium tetrafluoroborate and powders of a lithium borosulfate glass ($0.4B_2O_3 \cdot 0.4Li_2O \cdot 0.2Li_2SO_4$). The glass formation, properties and conductivity of numerous compositions in the Li_2O–B_2O_3–Li_2SO_4 system were measured and reported [6]. The room temperature conductivity of the $0.4B_2O_3 \cdot 0.4Li_2O \cdot 0.2Li_2SO_4$ glass has been reported to be around 10^{-6} S cm^{-1}. This glass composition was melted at 950 °C for 30 min, quenched, and ground to fine particles. The distribution of particle size of the glass ranged between 0.25 and 7.5 μm with the mean particle size around 1.5 μm. The concentration of PEO:$LiBF_4$ was adjusted such that the O:Li ratio remained constant at 8:1. The glass concentration in the composite electrolyte was varied from 0 to 19.17 wt.%.

Films containing the dopants were cast in a Teflon mold from solutions containing the components in the desired ratio in acetonitrile. The films were dried under partial vacuum at room temperature for 24 h. Several Li/PEO:$LiBF_4$-glass/Li and Li/PEO:$LiBF_4$-glass/Ni cells were assembled using the films. The cell fabrication technique consisted of assembling Li/film/Li laminate at a pressure of 100 psi and 70 °C, applying silver electrodes, and encapsulating in a polyethylene case. The cells were rectangular in size, varying in area from 2 to 5 cm^2. All the cells were annealed at 60 °C overnight and cooled down slowly to room temperature prior to experimental measurements.

The a.c. impedance measurement was conducted to characterize the electrochemical performance of the cells using an EG&G Princeton Applied Research model 368, a.c. impedance meter and a lock-in amplifier with a frequency range 0.1–100 kHz. The a.c. response of the Li/film/Li cells included two semicircles corresponding to high and low frequencies in the complex impedance plane. The high frequency semicircle relates to the bulk resistance, R_b, and bulk capacitance, C_b. The bulk resistance, R_b, was used to calculate the conductivity of the electrolyte materials. The second and low frequency semicircle reflects electrode/electrolyte interfacial resistance, R_e, and interfacial capacitance, C_e. The parameters, R_b and R_e, were used to calculate electrolyte conductivity, σ, and interfacial or charge-transfer resistance, ρ, as a function of

*Supplied by Union Carbide, average mol. wt. 300 000.

temperature, respectively. The cells were also characterized using an EG&G model 175 universal programmer coupled with a model 173 potentiostat/galvanostat. The microstructure of the composite electrolyte was evaluated using an International Scientific Instruments model SIIIA scanning electron microscope. Some of these cells were cycled for several hundred cycles with a half cycle of 1 h and a current of 50 μA at ambient temperature, 50, 75, 100 and 125 °C. During the cycling experiment, the voltage drop across the cell was monitored and recorded as a function of time and temperature. The voltage was then related to the electrochemical events taking place in the cell.

Results and discussion

Impedance spectroscopy

A typical complex impedance plot of a Li/composite/Li cell is shown in Fig. 1. Most of the specimens exhibited two semicircles. At high temperatures, due to the frequency limitation of the equipment, only a segment of the high frequency semicircle was obtained in some specimens. The electrolyte conductivity was determined from the intercept of the first semicircle with the z' axis. The electrode/electrolyte interfacial resistance, ρ, was determined from the diameter of the second semicircle.

The effect of the glass additive on the temperature dependence of conductivity is shown in Fig. 2. It should be noted that the addition of glass alters the slope of the log σ versus $10^3/T$ lines in the first three specimens. These lines are referred to as 1, 2 and 3 in Fig. 2, and they correspond to PEO:$LiBF_4$, PEO:$LiBF_4$-7.33% glass and PEO:$LiBF_4$-13.65% glass, respectively. The slopes of these lines reflect the associated activation energies. The calculated activation energies are 25.21, 26.91, and 30.00 kcal mol^{-1} for the curves marked as 1, 2 and 3, respectively. A further increase in the concentration of glass in the composite electrolytes to 19.17% decreases the conductivity with a small increase in activation energy to 31.01 kcal mol^{-1}.

The results obtained from the temperature dependence of the conductivity of these composite electrolytes differ from the data reported previously on polymer ceramic composite materials [4]. Capuano *et al.* [4] have reported an order of magnitude increase in the low temperature conductivity for small additions of γ-$LiAlO_2$ in PEO-based electrolytes. This study suggests that there is little effect of the glass additive on the conductivity. The small increase in the activation energy with the increasing concentration of glass is believed to be related to an enhancement of the potential

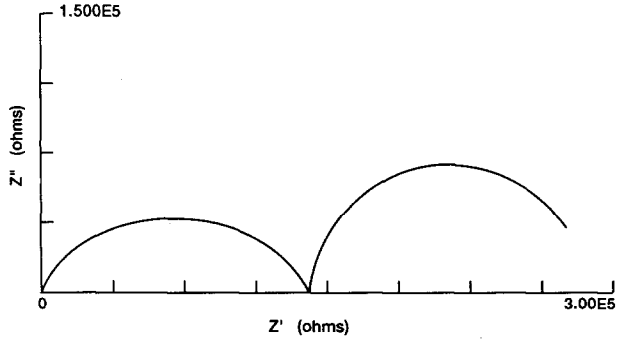

Fig. 1. Complex impedance plots of a Li/PEO:$LiBF_4$/Li cell at 10 °C.

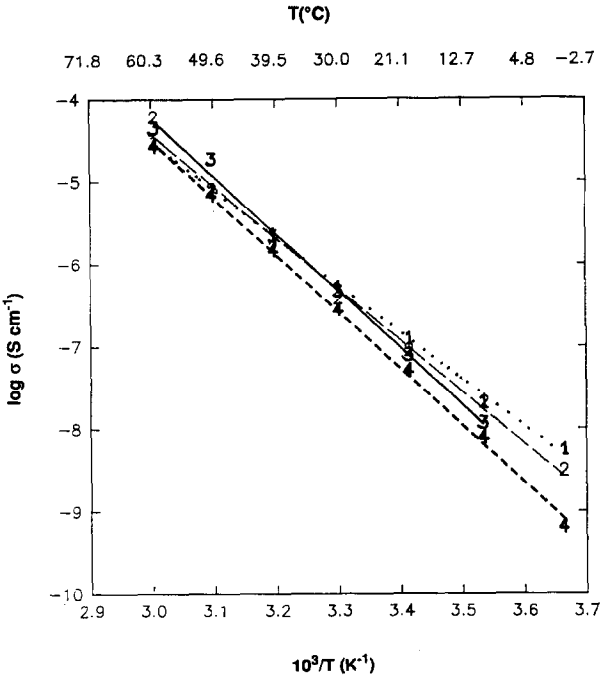

Fig. 2. Conductivity vs. temperature for various composite electrolyte: (1) PEO:$LiBF_4$, (2) PEO:$LiBF_4$-7.33% glass, (3) PEO:$LiBF_4$-13.65% glass, (4) PEO:$LiBF_4$-19.17% glass.

barrier in the path of the conducting ions that may result from either increased viscosity or a reduction in the segmental chain motion of the polymer.

Figure 3 shows the charge-transfer interfacial resistance, ρ, of Li/composite/Li cells as a function of temperature. The charge-transfer resistance also exhibits the Arrhenius type of behavior. The calculated activation energy for the charge-transfer resistance of the Li/PEO:$LiBF_4$/Li cells 24.73 kcal mol^{-1}. After the addition of glass to the PEO:$LiBF_4$ complex at 7.33, 13.65 and 19.17% levels, the activation energies changed to 23.76, 24.40 and 26.91 kcal mol^{-1}, respectively. It is thus inferred that the activation energy for a charge transfer in the first three specimens, i.e., PEO:$LiBF_4$, PEO:$LiBF_4$-7.33% glass and PEO:$LiBF_4$-13.65% glass, ramains constant at about 24.0 kcal mol^{-1}; however, there appears to be an increase in the activation energy for the PEO:$LiBF_4$-19.17 wt.% glass electrolyte to 26.91 kcal mol^{-1}.

A revealing feature of Fig. 3 is the significant reduction in the charge-transfer resistance after glass incorporation into the PEO:$LiBF_4$ complex. The charge-transfer resistance is reduced by a factor of 3 when 7.33% of the glass is incorporated into the PEO:$LiBF_4$ polymer. A further increase in the concentration of glass appears to have little effect. This feature of the composite electrolyte offers an advantage with respect to the cycle life and the overall performance of polymer cells. It is believed that the glass in the electrolyte enhances charge-transfer reactions at the electrolyte–electrode interface.

Cyclic voltammetry (CV)

Cyclic voltammograms of Li/composite/Li cells with a scan rate of 20 mV s^{-1} at 60 °C are shown in Fig. 4. It should be noted that the addition of the glass to the

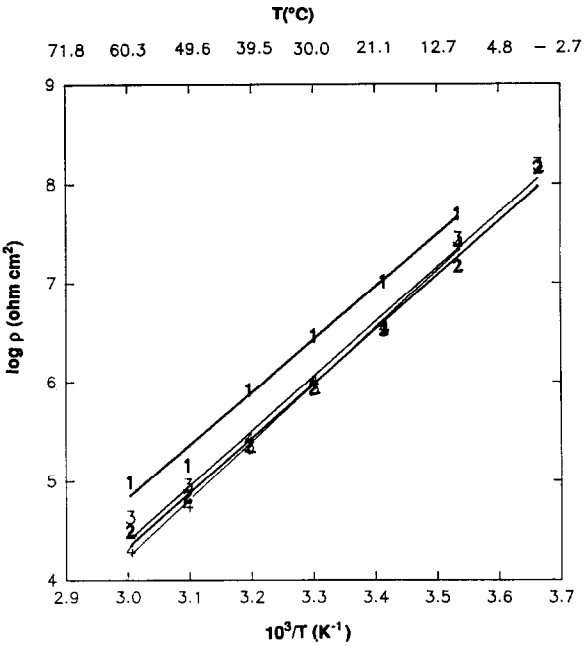

Fig. 3. Charge-transfer resistance as a function of temperature for various Li/composite/Li cells: (1) PEO:$LiBF_4$, (2) PEO:$LiBF_4$-7.33% glass, (3) PEO:$LiBF_4$-13.65% glass, (4) PEO:$LiBF_4$-19.17% glass.

PEO:$LiBF_4$ complex progressively decreases the peak potential difference, ΔE. PEO:$LiBF_4$ exhibits a ΔE of 3.8 V, and ΔE is decreased to 2.98 and 2.30 V for the composite electrolytes containing 13.65 and 19.17 wt.% glass, respectively. These data also suggest that the glass acts like an enhancer in lowering the potential at which electrode reactions take place. The presence of one cathodic and one anodic peak implies that the new constituents of the glass such as boron and sulfur are non-reactive to lithium.

The peak current, i_p, is also affected by the addition of glass; however, in this case the i_p goes through an optimum for 13.65 wt.% glass (Fig. 4(b)) and then decreases for 19.17 wt.% glass (Fig. 4(c)) to a value lower than that of the PEO:$LiBF_4$ complex. The enhancement of i_p for the 13.65% specimen is not clearly understood at the present time. The CV results of Fig. 4 substantiate the impedance data with respect to charge-transfer resistance and the catalytic effect of the glass additive. A repetitive cycling of Li/composite/Li cells exhibited only a small shift in the peak locations and intensities, suggesting a relatively efficient deposition and stripping of Li on the Li substrate.

A cyclic voltammogram of an Li/PEO:$LiBF_4$/Ni cell is shown in Fig. 5. The repetitive Li deposition and stripping processes on an Ni working electrode are characterized by a shift in the potentials of cathodic and anodic peaks. The locations and intensities of the peaks shift with the number of cycles, suggesting a rather significant passivation of the Ni substrate which leads to a decrease in the peak currents. The unsymmetrical shape of the curve indicates that the reversibility of the process is poor, which further implies that the lithium deposition on the cathode is not followed by an equivalent stripping of lithium at the anode.

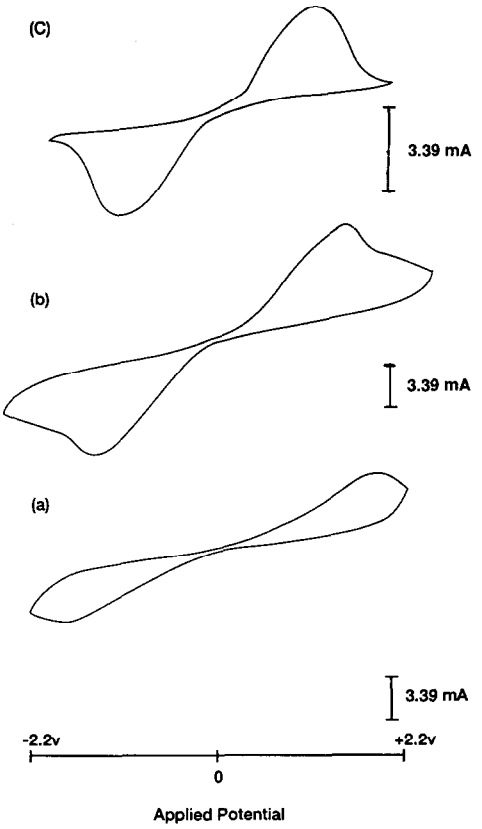

Fig. 4. Cyclic voltammogram of Li/composite/Li cells: (a) no glass, (b) 13.65 wt.% glass, (c) 19.17 wt.% glass; scan rate 20 mV s^{-1}, temperature 60 °C.

Charge/discharge cycling

Cell performance as a function of temperature

The charge and discharge curves of an Li/PEO:$LiBF_4$-7.33% glass/Li cell during the fifth cycle at ambient temperature and a 50 μA current are shown in Fig. 6. At the beginning of each half cycle, the cell exhibits a high voltage which decays exponentially. The voltage reaches a minimum value and then again it gradually increases until the half cycle ends. After a reversal of the current flow a similar trend in voltage variation was noted. The cycling data were identical for 150 complete cycles at the ambient temperature. Thus, there are two segments of the voltage curve that need to be explained in terms of electrochemical events that take place in the cell.

The initial high voltage and its exponential decay are attributed to a resistive or passivation layer at one of the electrode surfaces. This layer breaks up in about 3 to 5 min and the voltage reaches a minimum and then increases. This voltage increase is probably related to the depletion of the lithium available for transport and it may likely be a diffusion-controlled process. In such a situation, the inverse of voltage should show a linear dependence with the square root of time (see Appendix A).

A plot of $1/V$ versus $t^{1/2}$ a half cycle at ambient temperature is shown in Fig. 7. The latter part of the half cycle indeed shows a linear relationship adding

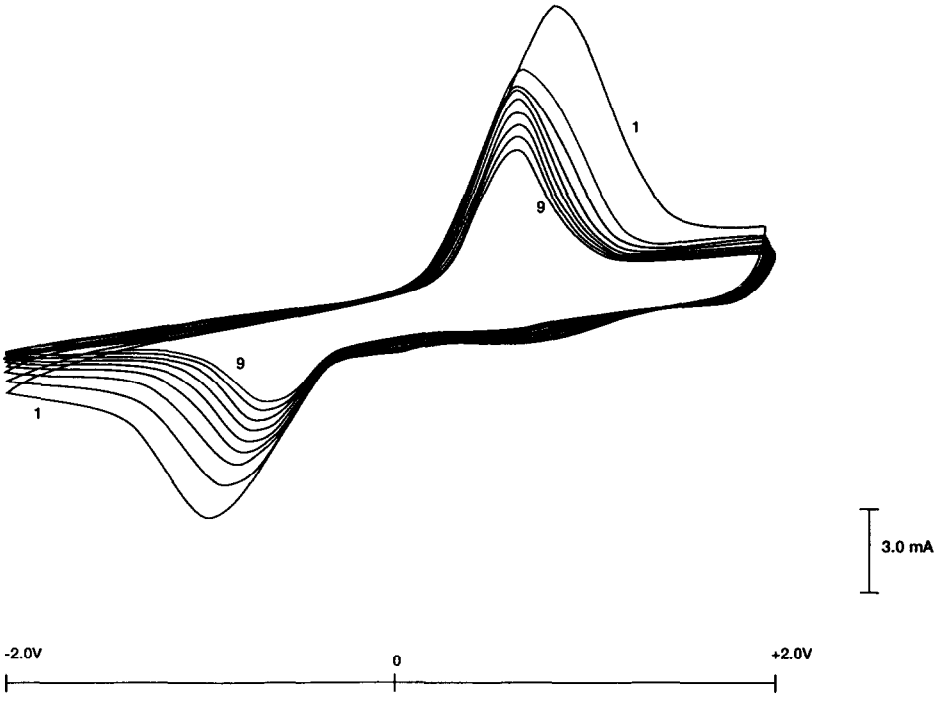

Fig. 5. Cyclic voltammograms of a Li/polymer/Ni cell, scan rate 20 mV s^{-1}, temperature 60 °C.

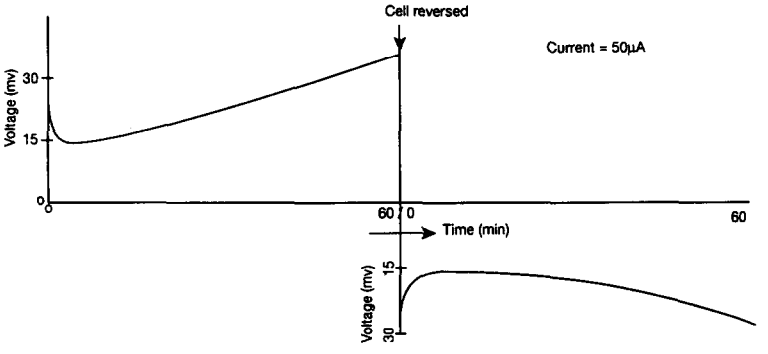

Fig. 6. Charge and discharge curve of a symmetric cell at ambient temperature. Electrode area = 6.45 cm^2. Film thickness = 0.0115 cm.

credence to our explanation that the electrochemical phenomenon drives the latter part of the charge and discharge curves at ambient temperature.

The charge and discharge curves were also obtained at 50, 75, 100 and 125 °C. The high initial voltage and its exponential decay within 3–5 min was a characteristic of the ambient temperature curves. This phenomenon was reduced to a certain degree when the specimen temperature was raised to 50 °C, and it completely disappeared at 75 °C, as shown in Fig. 8. All the charge/discharge curves at temperature $\geqslant$ 75 °C exhibit an exponential increase in voltage in the beginning, which is then followed by

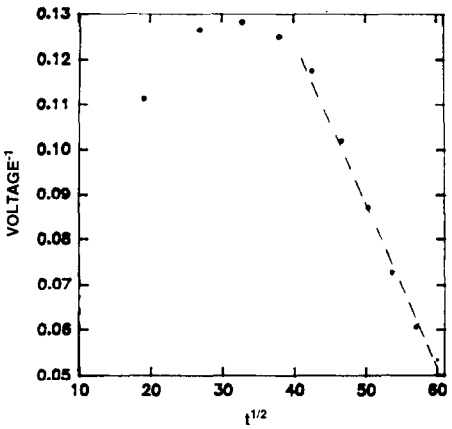

Fig. 7. $1/V$ vs. $t^{1/2}$ at ambient temperature of a Li/composite/Li cell.

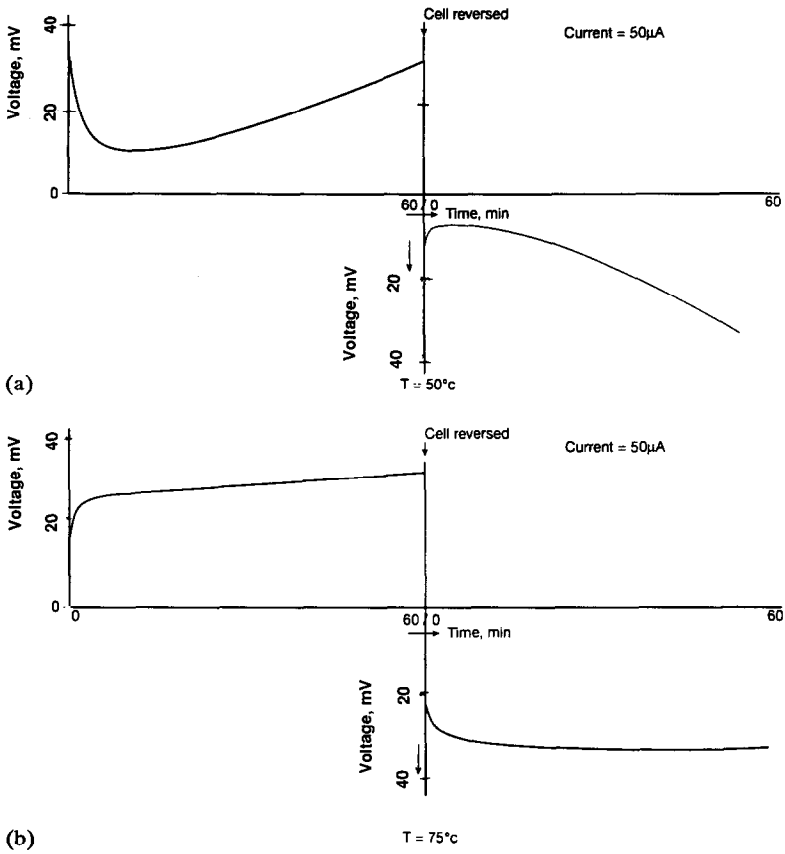

Fig. 8. Charge/discharge curves of a symmetric Li/film/Li cell at (a) 50 and (b) 75 °C. Electrode area = 6.45 cm^2. Film thickness = 0.0115 cm.

a more gradual increase. It is noted that the resistive layer that is formed at ambient temperature and is unstable at higher temperatures. This observation is consistent with the impedance data as presented in Figs. 2 and 3. The temperature dependence of the interfacial resistivity is greater than that of the temperature dependence of electrolyte resistivity. When the temperature is increased, beyond a certain value the only limiting factor is the electrolyte resistivity during the charge and discharge experiments. This temperature appears to be somewhere between 50 and 75 °C for this electrolyte. The melting point of the PEO:$LiBF_4$ complex ($\leqslant$68.2 °C) also happens to fall in this temperature range. It is thus believed that the disappearance of interfacial phenomenon may be related to the melting of the PEO:$LiBF_4$ complex.

A plot of V^{-1} versus $t^{1/2}$ for a half cycle at 75 °C is shown in Fig. 9. This Figure depicts a linear relationship during most of the half cycle. A deviation from the linear relationship is noted toward the end of the half cycle.

The temperature dependence study also revealed an increase in cell voltage with successive increases in the number of cycles, specifically at higher temperatures. This phenomenon was quite pronounced at 125 °C. A typical increase in cell voltage with an increasing number of cycles at 125 °C is shown in Fig. 10. Approximately a three-fold increase in cell voltage is observed after five cycles. This suggests that the resistance of the cell has increased approximately by three-fold. The increased resistance is believed to be related to the aging of the polymer electrolyte and/or the extensive reaction of lithium with the electrolyte.

A few of the cells were cycled for over 1500 cycles at ambient temperature with no obvious problem. Their charge/discharge characteristics remained similar to the one shown in Fig. 6. The cycling efficiency appeared to be excellent for these half cells with composite material as the electrolyte and two lithium electrodes.

Determination of the concentration (n_i), mobility (μ_i), and diffusion coefficient (D_i) of lithium

The charge and discharge experiments also allowed us to determine the concentration, n_i, mobility, μ_i, and diffusion coefficient, D_i, of the conducting lithium ions. Toward the end of a cycle in the experiment at 75 °C, external power to the cell was turned off and the polarized cell was allowed to relax. During the relaxation process, both current and voltage were recorded (Fig. 11(a)). The voltage and current curves

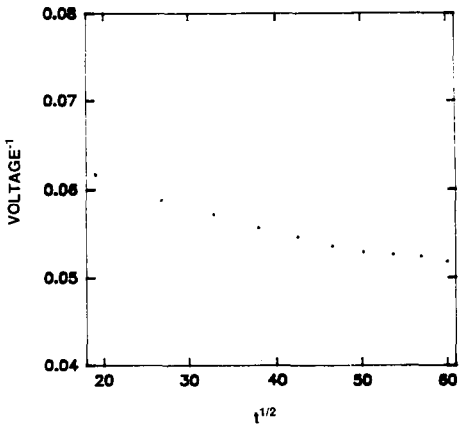

Fig. 9. $1/V$ vs. $t^{1/2}$ at 75 °C of a Li/composite/Li cell.

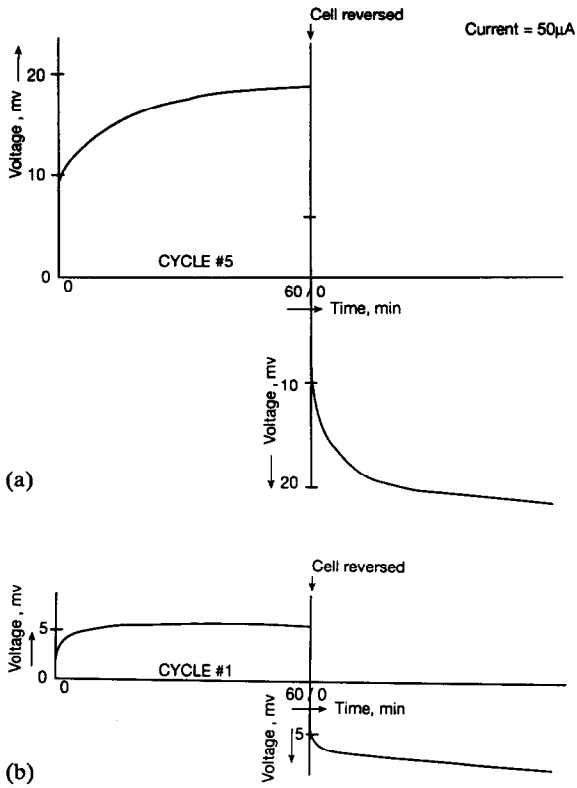

Fig. 10. Charge/discharge curves of a symmetric Li/film/Li cell at 125 °C: (a) after 5 cycles, (b) after 1 cycle. Electrode area = 6.45 cm^2. Film thickness = 0.0115 cm.

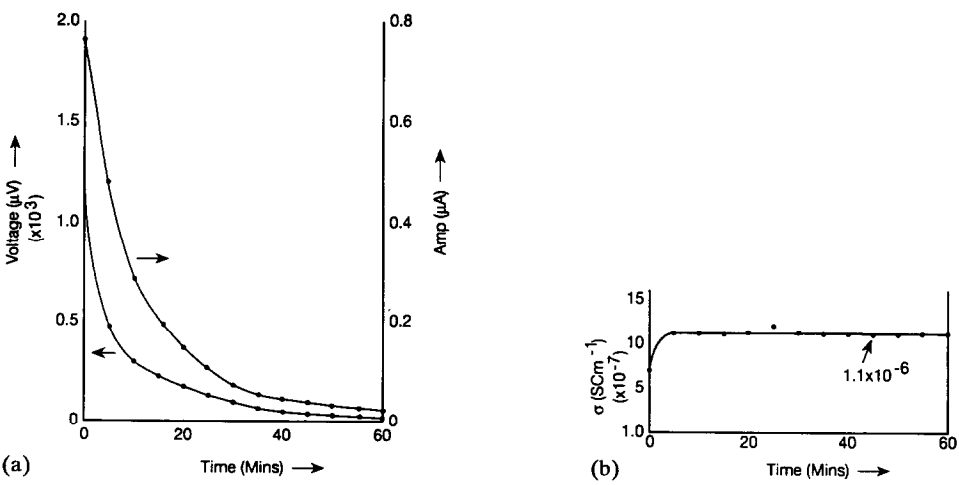

Fig. 11. (a) Voltage and current relaxation of a polarized cell at 75 °C. (b) Conductivity of the cell as obtained from the ratio of current and voltage, and cell geometry at 75 °C. Electrode area = 6.45 cm^2. Film thickness = 0.0115 cm.

are typical of the relaxation processes. From these voltage and current curves and the geometry of the cell, the conductivity, σ, of the cell was calculated and shown in Fig. 11(b). Ignoring the early part of the relaxation experiment, a reasonably constant σ with a value of 1.11×10^{-6} S cm^{-1} at 75 °C is obtained. This conductivity value is about two orders of magnitude lower than that of the value obtained by impedance spectroscopy (Fig. 2). This is expected because the potential barrier for the diffusion of lithium in the electrolyte is higher. The barrier is diminished by the application of voltage across the cell resulting in low activation energy and increased mobility. From Fig. 11(a) and (b), n_i was determined to be 3.33×10^{15}. The chemical diffusion induced conductivity in combination with n_i allowed the determination of mobility, μ_i. A value of 2.08×10^{-3} A(VcmC)$^{-1}$ was obtained. Further application of the mobility data yielded a value of $D_{Li}=7.49\times10^{-7}$ cm^2 s^{-1}. The calculated diffusion coefficient at 75 °C is comparable to the value reported for lithium self diffusion in $LiCF_3SO_3$-doped polyethylene oxide and measured by NMR spectrometry [7]. The calculation of n_i, μ_i, and D_i is shown in Appendix B.

Scanning electron microscopy (SEM)

Figures 12(a)–(d) show scanning electron micrographs of composite electrolyte specimens. On a scale of about 5–10 μm, the PEO:$LiBF_4$ specimen in Fig. 12(a) shows a relatively homogeneous microstructure and a crystalline morphology. A 3.8 wt.%

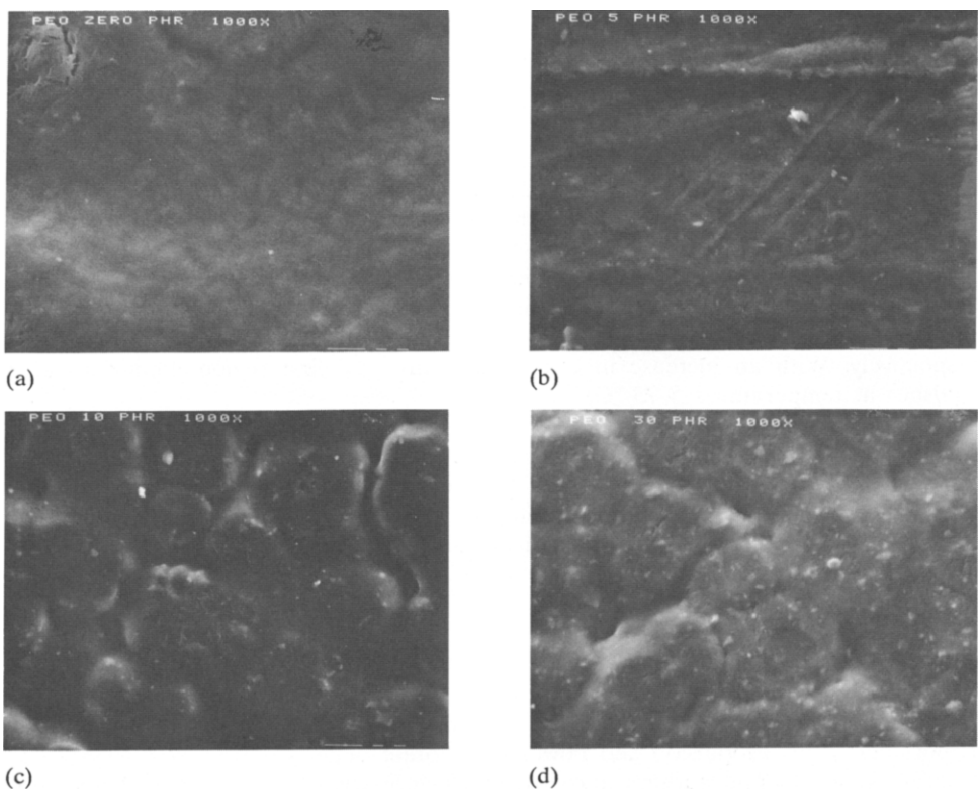

Fig. 12. Scanning electron micrographs of PEO:$LiBF_4$-glass electrolytes: (a) PEO:$LiBF_4$, (b) PEO:$LiBF_4$-3.80% glass, (c) PEO:$LiBF_4$-$LiBF_4$-7.33% glass, and (d) PEO:$LiBF_4$-19.17% glass.

glass addition changes this to a rather diffused morphology (Fig. 12(b)). The microstructure again becomes distinct for the 7.33 wt.% specimen (Fig. 12(c)) and remains similar for the 19.17 wt.% specimen (Fig. 12(d)). The glass particles are evident as brighter spots in these micrographs, and, as expected, their concentration increases on going from Fig. 12(b) to (d). It should also be noted that there is a distribution of glass particle size in the 0.5–2 μm range, as one would expect. The crystalline morphology of the 10–30 μm range is very much evident for the 7.33 and 19.17 wt.% specimens.

Summary and conclusions

Solid composite electrolytes from a PEO:$LiBF_4$ polymer complex and a lithium borosulfate glass were formulated and characterized using impedance spectroscopy, cyclic voltammetry, charge/discharge cycling and scanning electron microscopy. The analysis of these data led us to arrive at the following conclusions.

1. The temperature dependence data of the conductivity in the 0 to 60 °C range suggests that for small additions of glass up to 13.65%, there is little effect on conductivity. However, the activation energy for the conductivity increases. Further increases in the glass concentration decrease the conductivity of the composite material to the lowest levels.
2. The charge-transfer resistance of Li/PEO:$LiBF_4$/Li cells is decreased by a factor of three when glass is incorporated in the polymer. However, this phenomenon is independent of the concentration of glass in the composite electrolyte. The activation energy for charge transfer is around 24 kcal mol^{-1}, which shows only a slight variation among different materials.
3. The cyclic voltammetry data reveal significant variations in the anodic and cathodic peak potential as the composition of the composite electrolyte material was varied. The peak potential difference, ΔE, decreases with the addition of the glass. The glass acts like a catalyst to lower the potential at which the electrode reactions take place.
4. The charge and discharge curves of symmetric cells at temperatures below 75 °C show two distinct regions. The first and second regions are attributed to the formation of a resistive layer at the electrode and the depletion of lithium ions, respectively. With an increase in cell temperature, the first region diminishes and vanishes at temperatures $\geqslant 75$ °C.
5. At higher temperatures, the cell voltage increased with an increasing number of cycles. This phenomenon was enhanced as the cell temperature was increased.
6. The repetitive Li deposition and stripping on nickel substrate suggest significant passivation of nickel and poor reversibility.
7. The SEM micrographs show significant variation in the morphology of the composite material. Higher concentrations of glass in the composite material led to well-defined crystallite regions.

Acknowledgements

The authors gratefully acknowledge the financial support provided by the Wright Laboratory, Aero Propulsion and Power Directorate under Contract No. F33615-90-C-2036, Task 14. The authors also express their gratitude to Mr R.A. Marsh for continued support, encouragement, and constructive criticism and to John F. Leonard for assistance with scanning electron microscopy.

References

1 M.B. Armand, *Polymer Electrolyte Reviews – 1,* Elsevier Applied Science, Barking, UK, 1987, p. 1.
2 K.M. Abraham and N. Alamgir, *J. Electrochem. Soc., 137* (1990) 1657.
3 J.E. Weston and B.C.H. Steele, *Solid State Ionics, 7* (1982) 75.
4 F. Capuano, F. Croce and B. Scrosati, *J. Electrochem. Soc., 138* (1991) 191B.
5 B. Scrosati, *Proc. 35th Int. Power Sources Symp., Cherry Hill, NJ, USA, June 22–25, 1992,* pp. 267–270.
6 M. Yamashita and R. Terai, *Glastech Ber., 1* (1990) 13–17.
7 A.V. Chadwick and M. Worboys, *Polymer Electrolyte Reviews – 1,* Elsevier Applied Science, Barking, UK, 1987, p. 275.

Appendix A

Diffusion equation and its solution to determine voltage and time relationship in the cycling experiment

The depletion of lithium may be described by using Fick's laws of diffusion. The electrochemical response and characteristics of a symmetric cell as shown in Fig. A1 under a constant current or flux can be approximated by using Fick's second law of diffusion, eqn. (A1):

$$\frac{\partial C}{\partial t} = D \frac{\partial^2 C}{\partial x^2} \tag{A1}$$

The concentration, C, of diffusing species (Li in the present case) is a function of time, t, and distance, x.

To analyze the electrochemical response of the cell, one must solve the differential eqn. (A1) and describe how the concentration of diffusing species varies with time and distance after the constant flux or current is applied. $C(t=0)$ refers to the concentration before the commencement of ion transport, i.e. it describes the initial condition of the polymer electrolyte in which diffusion is made to occur by the flow of a constant current. The initial condition of the electrolyte is $C(t=0)=C^0$. The first boundary condition relates to a point very far from the boundary at which the diffusion

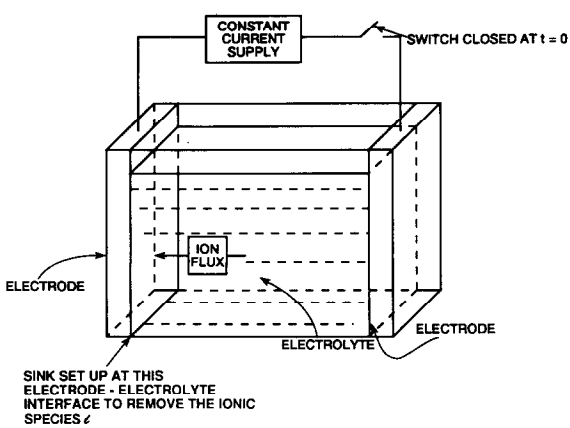

Fig. A1. Schematic of a symmetric cell with a constant flux.

source or sink is established. The concentration of the diffusing species at this point is unperturbed and remains the same as the initial condition, i.e. $C(x \rightarrow \alpha) = C(t=0) = C^0$. The second boundary condition states that at any instant of time, the concentration flux across the boundary is related to the concentration gradient through Fick's first law, i.e.:

$$J_{x=0} = 1 = -D\left(\frac{\partial C}{\partial x}\right)_{x=0}$$

The boundary conditions can be summarized as:

$$C[t=0] = C^0 \tag{A2}$$

$$C[x \longrightarrow \alpha] = C^0 \tag{A3}$$

$$\left(\frac{\partial c}{\partial x}\right)_{x=0} = \frac{1}{D} \tag{A4}$$

The solution of eqn. (A1) is facilitated by introducing a new variable, C_1, such that:

$$C_1 = C^0 - C \tag{A5}$$

The variable C_1 can be recognized as the difference $(C^0 - C)$ of the concentration from its initial value, C^0. In other words, C_1 represents a perturbation from the initial concentration. The partial differential eqn. (A1) and the initial boundary conditions can now be restated in terms of the new variable, C_1:

$$\frac{\partial C_1}{\partial t} = D\frac{\partial^2 C_1}{\partial x^2} \tag{A6}$$

$$C_1(t=0) = 0 \tag{A7}$$

$$C_1(x \longrightarrow \alpha) = 0 \tag{A8}$$

$$\left(\frac{\partial C_1}{\partial x}\right)_{x=0} = \frac{1}{D} \tag{A9}$$

After Laplace transform, the differential eqn. (A6) becomes:

$$p\bar{C}_1 - C_1[t=0] = D\frac{\mathrm{d}^2\bar{C}_1}{\mathrm{d}x^2} \tag{A10a}$$

since $C_1[t=0] = 0$

$$\frac{\mathrm{d}^2\bar{C}_1}{\mathrm{d}x^2} = \frac{p}{D}\bar{C}_1 \tag{A10b}$$

The general solution of the equation has the following form:

$$\bar{C}_1 = A\exp(-(p/D)^{1/2}x) + B\exp(p/D)^{1/2}x \tag{A11}$$

Since $\bar{C}_1(x \rightarrow \alpha) = C^0$, therefore $\bar{C}_1(x \rightarrow \alpha) = 0$; this will only be true if $B = 0$. Therefore:

$$\bar{C}_1 = A\exp(-(p/D)^{1/2}x) \tag{A12}$$

Differentiating eqn. (A12) with respect to x:

$$\frac{d\bar{C}_1}{dx} = -\sqrt{\frac{p}{d}} A \exp(-(p/D)^{1/2}x)$$

at x=0

$$\left(\frac{d\bar{C}_1}{dx}\right)_{x=0} = -\sqrt{\frac{p}{d}} A \tag{A13}$$

It can also be shown by Laplace transform of eqn. (A9) that:

$$\left(\frac{d\bar{C}_1}{dx}\right)_{x=0} = \frac{1}{D} \tag{A14}$$

Thus,

$$A = \frac{1}{p^{3/2}D^{1/2}}$$

and,

$$\bar{C}_1 = \frac{1}{p^{3/2}D^{1/2}\exp(-(p/D)^{1/2}x} \tag{A15}$$

An inverse transform of eqn. (A15) gives rise to an equation for C_1 such that:

$$C_1 = \frac{1}{D^{1/2}}\left[\frac{2t^{1/2}}{\pi^{1/2}\mathrm{e}}\left(\frac{x^2}{4Dt}\right) - xD^{1/2}\mathrm{erfc}\left(\frac{x^2}{4Dt}\right)^{1/2}\right] \tag{A16}$$

where erfc is the error function complement defined by

$$\mathrm{erfc}(y) = 1 - \mathrm{erf}(y) \tag{A17}$$

and,

$$\mathrm{erf}(y) = \frac{2}{\sqrt{\pi}}\int_0^y \exp(-u^2)\mathrm{du} \tag{A18}$$

In the case of an electrochemical cell, where the electrolyte thickness is very small, one can further impose a condition that $x \to 0$. Then:

$$C_1 = \frac{2}{\sqrt{\pi D}} t^{1/2} \tag{A19}$$

$$C = C^0 - \frac{2}{\sqrt{\pi D}} t^{1/2} \tag{A20}$$

Equation (A20) describes the change in concentration of diffusing species at the sink or source. In our experiment, we have measured the change in voltage at a constant current or flux. The voltage variation is related to the conductivity of the cell which in turn is directly related to the number of charge carriers, i.e. concentration of lithium ions. In other words, the voltage is inversely proportional to the concentration of lithium ions which is the limiting factor at either the source or the sink such that:

$$\frac{K}{V} = C \tag{21}$$

where K = constant.

Combining eqns. (A20) and (A21), one obtains:

$$\frac{1}{V} = \frac{C}{K} = \left(\frac{C^0}{K}\right) - \left(\frac{2}{K\sqrt{\pi D}}\right) t^{1/2} \tag{22}$$

Equation (A22) is a basic equation showing how the voltage varies with the time, t, that has elapsed since a constant flux was established. A plot of $1/V$ versus $t^{1/2}$ should yield a straight line for a truly diffusion controlled electrochemical reaction taking place either at the source or the sink. The intercept and slope determine the initial concentration and D_{Li}, respectively.

Appendix B

Calculation of concentration, n_i, mobility, μ_i, and diffusion coefficient, D_i, from the relaxation data

$$n_i = \frac{\mu\text{Ah} \times 10^{-3} \times N}{3898.5 \text{ mAh g}^{-1} \times 6.94} = \frac{0.14982 \times 10^{-3} \times 6.02 \times 10^{23}}{3898.5 \times 6.94}$$

$$= \frac{14982 \times 6.02}{3898.5 \times 6.94} \times 10^{15} = 3.33 \times 10^{15}$$

$$\mu_i = \frac{1.11 \times 10^{-6}}{n_i z_i e} \frac{\text{A}}{\text{VcmC}} \qquad \left[= \frac{\sigma}{n_i z_i e} \right]$$

$$= \frac{1.11 \times 10^{-6}}{3.33 \times 10^{15} \times 1.602 \times 10^{-10}}$$

$$= 2.08 \times 10^{-3} \frac{\text{A}}{\text{VcmC}}$$

$$D_i = \frac{\mu_i}{2_i e} kT$$

$$= \frac{2.08 \times 10^{-3}(\text{A}) \times 1.381 \times 10^{-23}(\text{J K})^{-1} \times 348 \text{ K}}{1.602 \times 10^{-19}(\text{VC}^2 \text{ cm})}$$

$$= 6.24 \times 10^{-5} \frac{\text{AC}^{-1}\text{J}}{(\text{VC})\text{cm}}$$

$$= 6.24 \times 10^{-5} \text{ cm}^{-1} \text{ s}^{-1} [\text{AC}^{-1} \cong \text{s}^{-1}]$$

$$D_i = 6.24 \times 10^{-5} \times 0.012 \text{ cm}^3 \text{ cm}^{-1} \text{ s}^{-1} \qquad (D_i \times \text{vol. of the film})$$

$$= 7.49 \times 10^{-7} \text{ cm}^2 \text{ s}^{-1}$$